Phase Doppler Interferometry for Efficient Cloud Drop Size Distribution, Number Density, and LWC Measurements

William Don Bachalo, Gregory Payne, Khalid Ibrahim, and Michael Fidrich
Artium Technologies Inc.

Abstract

Threats to aviation safety as a result of super-cooled large drops (SLD) has been addressed by the FAA rules change (14 CFR Part 25) with the additional icing certification requirement. SLD clouds often consist of bi-modal drop size spectra leading to significant problems in simulating and characterizing these conditions in situ and in icing wind tunnels. Legacy instrumentation for measuring drop size distributions and liquid water content are challenged under these conditions. The large size range measurement problem is addressed with the development of the Phase Doppler Interferometer, Flight Probe Dual-Range (PDI FPDR). The method is described in this report along with the measurement capabilities including the dynamic measurement range and overall working size range. The PDI instrument bases drop size measurements on the light wavelength as the measurement length scale. The light wavelength is a much more robust scale, especially as compared to the light scattering intensity. Methods for accurately characterizing the sample volume in situ based on measured drop velocity and transit time are reviewed, given the importance of this parameter for merging results and measuring LWC. Droplet coincidence in the sample volume can be problematic so this condition is treated with an innovative signal parsing approach. Measurement examples acquired in the NASA IRT are provided. Measurements of LWC showed good agreement with the Artium Particle Imaging (PI) instrument but diverged from the tunnel calibration results for larger MVD values.

Introduction

The FAA's rule change (14 CFR Part 25) for super-cooled large drops (SLD) conditions mandates testing under spray conditions that are difficult for icing certification test facilities to generate. SLD clouds have been found to contain bimodal drop spectra [2] that can be quite difficult to reproduce in an icing tunnel with current spray nozzle technologies. Research has been underway at several icing wind tunnel facilities to develop suitable test conditions. To simulate SLD conditions, the spray nozzles must reproduce the natural cloud drop distributions reasonably well, and the drops must approach thermo-kinetic equilibrium with the airstream by the time they reach the test section. Furthermore, the contraction section influences droplet slip (relative velocity between the droplet and air flow) and trajectories according to the drop inertial parameters [4] which may be complicated due to shape deformation.

Accurately measuring SLD icing conditions in research flights and in experimental facilities is a critical requirement for developing a sound basis for aircraft component Appendix O certifications. Exacerbating the difficulty in simulating icing cloud conditions is an apparent lack of verified instrumentation optimized for the required large drop size range conditions containing large droplets (median volume diameters between 100 and 500 μm) and bimodal diameter distributions. Under these conditions, it is challenging to establish that the research facilities are generating the targeted diameter/velocity distributions while ensuring that the droplets at the test location are supercooled. Instrumentation assessment and development has been identified as a major technical study area for SLD engineering [6]. Prior wind tunnel measurement assessments of data uncertainty have been reviewed in AGARD No. 304 and AIAA Standard S-071A-1999. SAE-ARP 5905 stipulates that icing testing should be performed in facilities with measured, defined, and documented aero-thermodynamic flow qualities, icing cloud qualities, and calibrated instrumentation for Appendix C. No assessments or recommendations of acceptable instrumentation for this purpose have been given. Currently, calibrations are not based on absolute reference values which could lead to inter-facility biases due to the use of different calibration instrumentation. This is particularly problematic for SLD measurements, where significant problems have been documented with certain instruments, and in general there have been few studies of the comparability of the different technologies for median volume diameter (MVD) and liquid water content (LWC) measurements. Consequently, ice shapes generated from a given set of nominal conditions, especially for MVDs higher than 30 μm, cannot be expected to reproduce from one tunnel to another, even if the tunnel calibrations were technically in compliance with SAE-ARP 5905.

Over the past four decades, atmospheric clouds and wind tunnel simulation measurements of icing conditions have relied primarily on instruments based on the design of the FSSP [1] and 2D Cloud Optical Array Probes or their derivatives (e.g., DMT CIP, SPEC 2DS). The FSSP approach infers particle size from the pulse amplitude of scattered light resulting from the passing of a droplet through a focused laser beam. Typically, the FSSP approach is limited to spherical drop sizes in the range of 2 to 50 μm with their updated variants *(e.g., DMT CDP, DMT CASP, SPEC FCDP)* able to measure in a range of 2 to 95 μm.

Some of the deficiencies in the Droplet Measurement Technologies Cloud Droplet Probe (DMT CDP) method have been outlined, for example, by [10] and [11]. Faber et al. indicate that the CDP produced measurement errors and drop sizing that depended both on the diameter and position within the sampling area through which the

droplets transit. This effect was also analyzed in detail by [10]. The authors indicated that for smallest diameter droplets, the CDP undersize the droplets by 1 to 4 µm. For larger drops, it was found that the majority of drops were oversized by 2 to 4 µm.

The OAP-based methods use a linear array to reconstruct particle images by rapidly scanning the particles as they pass the sample volume. The more recent instruments based on this method utilize 64 or 128 photodiode arrays and are expected to size particles in the approximate range of 25 to 1550 µm. However, optical array probes have been reported to have image quality problems reducing the accuracy of measurements of drops smaller than about 35 µm (e.g., out-of-focus image errors, digitization errors, depth of field uncertainty; references [12], [13]), making them particularly problematic for measuring MVDs in the 30-100 µm size range. More recently, measurements of drop size versus velocity indicate substantial velocity lag (slip velocity) and droplet deformation for large drops in wind tunnels. This will complicate the sampling analyses for the line scan methods (OAP, 2DS, etc.).

To address cloud droplet size measurement requirements in the 1 to 2200 µm range, phase Doppler interferometry has been beneficial. The measurement principle is based on light scattering interferometry, which utilizes the wavelength of light as the measurement scale [14], [15]. This confers the PDI with many advantages, primarily, a very large measurement range, significantly improved performance under conditions of dense particle fields, resistance to contaminated optics, insensitivity to electronic drift, and noise, and a significantly reduced need for frequent calibration. Given the variability in measurement conditions, the instrument has been designed to respond by adjusting the measurement parameters to the prevailing cloud conditions including changing the size range sensitivity and sample volume size automatically. In the following sections, the method will be described in sufficient detail to enable the reader to understand the measurement principle and its capabilities. A description of the particle detection system and in situ sample volume characterization is provided. Examples of recent measurements acquired in the NASA IRT are provided to emphasize the capabilities of the PDI dual-range flight probe.

Experimental Methods

For these experimental studies, the phase Doppler interferometry method was used to acquire drop size distributions, LWC, and particle velocity response associated with SLD conditions.

Phase Doppler Interferometer

The phase Doppler interferometry technique evolved from the initial invention [14] and has been described in detail [15]. The measurement principle for this instrument is based on the concept of light scattering interferometry introduced by Bachalo [14]. With this approach, droplet size measurements utilize the wavelength of light as the measurement scale, in contrast to methods that utilize light scattering intensity. This approach has a number of advantages. In particular, the measurements are relatively insensitive to variations in the laser beam intensity, light scatter detection system, and changes in the detector amplitude response. The approach utilizes off-axis light scatter detection which has the significant advantage of allowing precise control of the probe volume size over which the particles may be observed. By utilizing an appropriate laser beam diameter at the sample volume and a selectable range of apertures in the receiver, the sample volume may be adapted to the prevailing droplet concentrations to both maximize data rate and minimize coincidence errors.

The basic optical configuration for the phase Doppler interferometer (PDI) is shown in Fig. 1 and consists of a single mode diode pumped solid state (DPSS) laser, a Bragg cell for frequency shifting and splitting the laser beam, and transmitting optics used to converge and focus the two laser beams to form the probe volume. The receiver system is located at a suitable off-axis angle, θ (30° to 40°), and consists of a segmented receiver lens, a slit aperture with selectable slit widths, and three photomultiplier tube detectors. Advantages of the selectable slit aperture are described in later sections. Droplets passing through the intersection of the laser beams scatter light with a sinusoidal frequency as a result of passing the interference fringes formed at the beam intersection. The temporal frequency of the scattered light is relatable to the droplet velocity which is based on the well-known laser Doppler velocimetry method. The spatial wavelength of the scattered sinusoidal pattern is inversely proportional to the droplet diameter as described by Bachalo, 1980. The signal produced by each of the three detectors consists of a Gaussian-shaped envelope with a high-frequency (Doppler component) superimposed. Signals simultaneously provide information for measuring droplet size, velocity, residence time, and time of arrival for each droplet passing the measurement volume. With modern electronics processing, droplet rates up to 100,000 per second or greater may be measured.

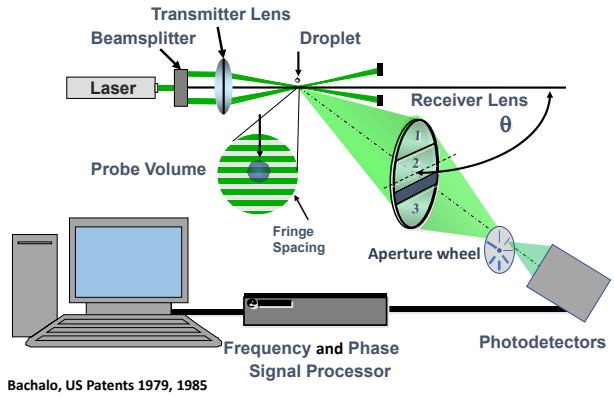

Figure 1: PDI system schematic showing the key components.

For a dynamic of range 50 to 1, the light scattering signal amplitude will vary proportional to the droplet diameter squared which results in the signal amplitude range of 2500 to 1. With the presence of noise, the smaller droplets may be easily missed, and noise spikes can be misinterpreted as small droplet signals. A significant advantage of the PDI method is that valid signals have a sinusoidal character which are easily discriminated from noise spikes. Digital detection systems have been invented [16] and introduced into the PDI instruments allowing reliable uniform measurements over the entire drop size range, even when the signal-to-noise ratio (SNR) is less than one. Reliable signal detection and accurate signal duration measurements are essential for characterizing the sample volume.

The PDI method is capable of measuring droplets over a size range of 0.5 to 2200 µm in diameter or larger, if the drops remain quasi-spherical. However, to accommodate the size range the optics must be designed to accommodate each measurement range. For smaller particles (e.g., 1 to 150 µm), the focused beam diameter of approximately 200 µm is typical, whereas for larger drops (e.g., 50 to 2200 µm) a beam diameter of approximately 2000 to 3000 µm is used.. Generally, a working range at one optical configuration will accommodate a size range of 1 to 150. The dynamic size range measurable at one detector gain setting is approximately a factor of 1

to 50 within the working range. The dynamic range can be adjusted within the working range by changing the detector gain. The signal amplitude is monitored, and the detector gain adjusted to optimize for the prevailing size distribution.

Different clouds and drizzle with SLD may be experienced on a specific flight operation and experiment. Selecting the appropriate drop size measurement range of interest a priori may be difficult or impossible if all conditions are to be covered, including SLD. Making adjustments to the size range of instruments could require significant effort and expertise on the ground before resuming the in-flight measurements and could lead to errors. To overcome this drawback, a dual-range PDI cloud probe has been developed that can cover an exceptionally wide drop size range from 1 to 2200 µm or larger. This probe design essentially involves the incorporation of two PDI instruments into one compact package. Combining the two measured size distributions is a nontrivial task and required dealing with optimization of the sample volume size, coincidence, and refinement to the size distribution merger algorithm.

Sample volume

An important advantage of the PDI method is that the light scatter detection uses a large off axis angle, θ, which subtends a well-defined length along the laser beam allowing easy adjustment of the sample volume size (Fig. 2). Computer controlled selections of slit aperture widths in the receiver driven by a statistical algorithm to estimate coincidence are used to adjust the length, and hence, the size of the sample volume (Fig. 3). The diameter of the laser beam at the sample volume can also be optimized to address the characteristics of the particle field to be measured. For small drop measurements, a more highly focused laser beam is used whereas for large drops, laser beam diameters of up to 3000 µm or larger may be used (Fig. 4).

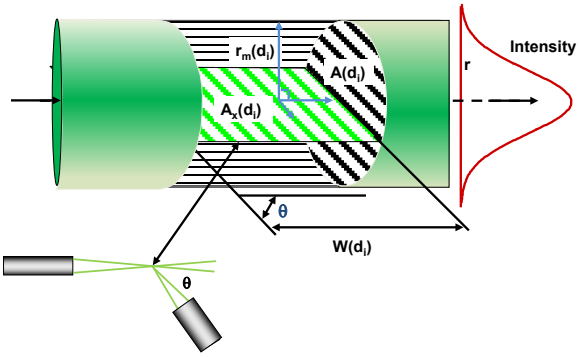

Figure 2: Schematic of the PDI sample volume is defined by the diameter of the laser beams and the slit aperture in the receiver.

Due to the Gaussian beam intensity profile, the effective diameter of the sample volume will be dependent upon the droplet size. As described in previous publications [15], [18] the effective diameter as a function of particle size is measured using the particle transit time recorded by the instrument and the measured particle velocity to define the path length. Since the sample volume is circular, there will be a range of path lengths for each size class depending upon their trajectory through the laser beam. The maximum path length for each droplet size defines the effective sample volume diameter or cross-section for that droplet size. In Fig. 5, the sample volume diameter for the size ranges is displayed. Each dot on this figure represents the droplet measurement probe volume (PV) length versus diameter. For the dual-range instrument (Fig. 6), the maximum lengths for the small and large size ranges are fitted with the theoretical curve which defines the sample volume diameter as a function of drop size for the two measurement ranges, green for the small and blue for the large size range.

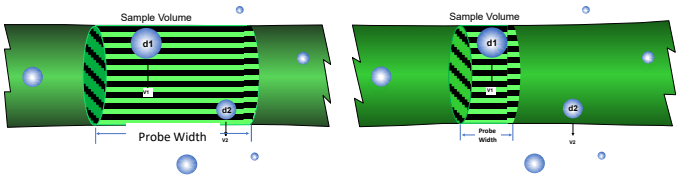

Figure 3: Schematic showing the sample volume delineated by the laser beam and the image of the aperture in the receiver which limit the length of detection along the laser beam. The sample volume is easily reduced by the software selectable slit apertures.

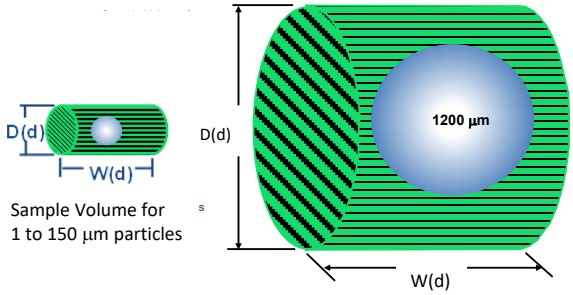

Figure 4: Schematic showing the sample volume sizes with the small and large size range respectively.

The length along the beam is defined by the image of the slit aperture. These apertures are software selectable and can be used to optimize the size of the measurement volume for the prevailing spray conditions.

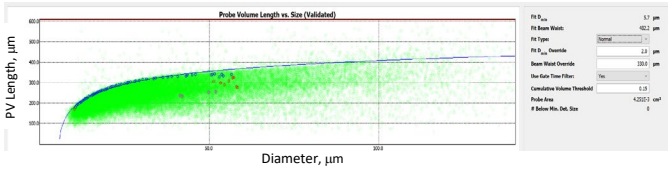

Figure 5: Plot the sample volume diameter versus droplet diameter for the small size range, measured in situ.

Coincidence

For efficient sampling of prevailing cloud conditions, the sample volumes for both the small and large size range should be as large as possible. However, given the Poisson statistical distribution of particle arrivals, coincidence events will inevitably occur. The problem is exacerbated by the need to have a much larger sample volume for the large size range and overlap in the measurement range to ensure completeness in the size distribution measurements. The detector gain for the small size range is set to ensure detection of the smallest drops of interest. The detector gain for the large size range is set to minimize the detection of the high population of small drops which would lead to significant coincidence. However, the probability of coincident events is still significant, so other measures are required to minimize this problem.

An estimation of the probability of having coincident measurements (more than one particle in the sample volume at one time) is provided using a Poisson statistical analysis. The probability of finding n particles within the probe volume V can be expressed as follows:

$$P(n)=\frac{(VN)^n}{n!}e^{-(VN)} \qquad (1)$$

where V is the sample volume size and N is the particle number density. Using this expression, the probability of finding only a single particle ($n = 1$) within the probe volume can be expressed as:

$$P(1) = (VN)\, e^{-(VN)} \qquad (2)$$

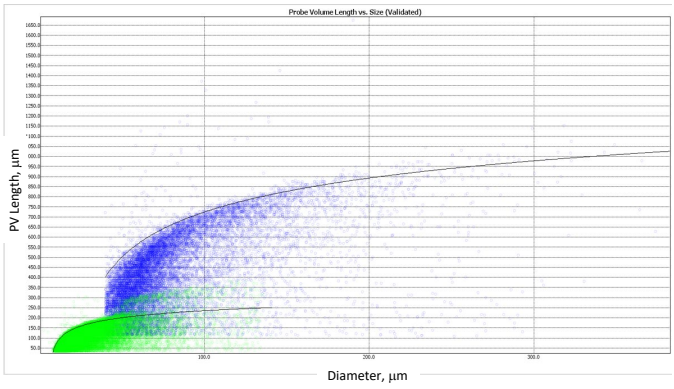

Figure 6: Plot of the sample volume diameters for the small (green) and large (blue) measured in situ.

An example of the variation of P(n) for coincidence events is shown in Fig. 7. One might assume that the probe volume, number density product, VN, providing the maximum probability P(1) for one particle in the probe volume would represent the optimum condition. However, as seen in Fig. 7, the probability of two particles, P(2) in the probe volume is significant at that condition (VN product) indicating the probability of coincidence is relatively high. Further reduction of the sample volume V decreases the data rate with the probability of P(0) increasing exponentially as shown by the green line on this plot. The goal is to maximize the P(1)/P(2) ratio to achieve an acceptably low probability of coincidence. From this plot, it is evident that even with a very small VN product, there remains a significant probability of coincidence. Furthermore, the required small sample volume, V will require much longer sample times to acquire acceptable statistics, especially for the largest drops in the size distribution. For in-flight cloud characterizations, there is interest in obtaining a statistically representative size distributions over relatively short distances to characterize the spatial variations in the cloud. This will also require additional measures to deal with the coincidence problem.

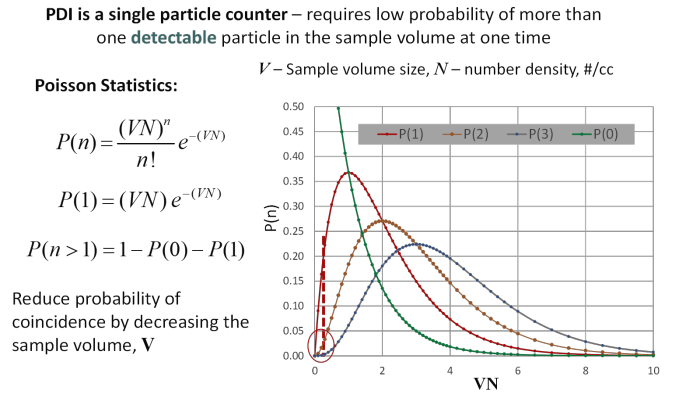

Figure 7: Probability for coincidence based on Poisson statistical analysis.

Signal Parsing

Signal processors for PDI applications require Doppler burst signal detection systems to detect and record the random arrivals of particles that produce Doppler signals. These detection systems must be capable of reliably detecting signals over a very wide dynamic amplitude range and should not produce significant false detections due to noise. A method for signal burst detection based on SNR using a real time Fourier transform approach was introduced [16] that facilitated reliable detection of Doppler signals with SNR down to 0 dB or lower without the need for user intervention, as was the case for the existing analog threshold voltage level detection methods. More recently an advanced method for digital detection was introduced [17] which allows the use of 32 or more complex digital samples for signal detection. The signal detection is based on the continuous digital sampling of the analog signals from phase Doppler detectors. These signals are sampled in quadrature and the quadrature signals are continuously analyzed for SNR. When a coherent signal is detected (SNR rises above a predetermined level), a burst detection gate is set (green square wave curve in Fig. 8), and that portion of the record is transferred to the computer for higher level processing using the full complex discrete Fourier transform (DFT). It is important to recognize that for sprays with a size range of 33 to 1, for example, the signal amplitude range is approximately 1000 to 1 so the smallest droplets will produce very small signals with low SNR.

In the center frame of Fig. 8, the first image shows two nearly contiguous signals that are detected individually as seen by the gate signals (green squares). In the center image, there are two leading signals that are partially overlapped and detected as a single event. This is a coincident detection. For such conditions, the signal is detected as a single event showing up as a filtered signal (magenta color) but remains coherent over the duration of both signals. Once processed using full complex Fourier transforms, the signal may be rejected if the phase shift and frequency are not consistent over the entire signal duration. It is also possible that the signal is accepted but reports an erroneous size. In the right frame, three signals arrive in quick succession with the burst detection system remaining active over the three signals. Once again, with conventional signal processing, these three signals would be analyzed using the full complex Fourier transform and rejected because of inconsistency in frequency and phase over the duration of the detected signal. Under more dense spray conditions and/or using larger sample volumes, detection of multiple particles as a single event will lead to a high degree of signal rejection and sampling bias towards the larger particles. Often, these conditions occur without the knowledge of the experimenter and the measurements are reported as valid. Clearly, even the most advanced signal detection means can be defeated under such conditions.

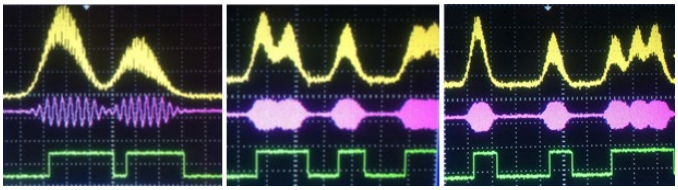

Figure 8: Three examples of signal detection for dense sprays. Yellow trace is the raw signals, the magenta trace is the down-mixed, high pass filtered, log amplified signal, and the green trace is the signal detection.

The coincident signals can be separated using a number of criteria [19]. With this approach, entire signals under the detection gate (green square wave) are recorded digitally with up to a hundred thousand ADC sample capability. When the detection gate remains active over more than one signal as seen in the middle and rightmost photos in Fig.

8, the combined signals are recorded. At the same time, the signal amplitudes are digitized with 12-bit amplitude quantization. To separate the signals, the peak amplitudes may be used as a guide to identify the number of coincident particles in the recording. Signal parsing is implemented by iteratively reprocessing the sampled digital replicas of the detected event using a number of strategies. This can be done in near real time or in post-processing. The Fourier transform is applied to discrete sequential sample segments of the signal to identify changes in the SNR, frequency, and phase of the signal segments. Where the signals overlap, the coherence of the signal will be compromised and that reduces the SNR, leading to rejection of that time segment. In addition, the frequency and phase shift will indicate where one signal overlaps the other. Saved ADC samples of the segments may be evaluated iteratively at varying lengths to identify the beginning and end of the individual signals while discarding the overlap region where measurements can be ambiguous. Once separated, the accepted segments are then used to establish the drop size and velocity of the coincident particle events.

This approach has been demonstrated to be reliable by forcing coincidence as shown in Fig. 8 using our monodisperse drop generator with larger sample volume diameters. Experimentation has been conducted to evaluate the methods of parsing signals to determine how well coincident signal events can be separated and whether this approach can significantly improve the validation rate, eliminate false large particle measurements, and improve on droplet number density and volume flux estimations. The general approach is currently under active development and evaluation.

Merging Results

For SLD conditions, ideally, instrumentation must be able to measure drop sizes over a size range of from 2 to 2200 µm or greater. For the legacy instruments, this generally requires the use of different optical methods which included light scattering intensity measurements (e.g., FSSP, CDP, etc.) and the line scan imaging approach (OAP, 2DS, etc.). The PDI method is unique in terms of having the capability of measuring the entire size range using the same measurement principle, namely, light scattering interferometry. However, as stated above, the entire size range needs to be either measured sequentially or simultaneously using two instrument measurement ranges, one for the small (1 to 150 µm) and one for large (50 to 2200 µm) drops. Merging distributions using fundamental principles, droplet flux measurements are needed, defined as:

$$VolumeFlux = \frac{\pi/6 D_{30}^3 * N}{PA * t_{total}} \quad (3)$$

where D_{30} is the volume mean diameter defined in Equation 4 where N is the number of drops measured, D_i is the diameter of the individual drops, PA is the probe cross sectional area, and t_{total} is the sample time:

$$D_{30} = \left(\frac{\sum N_i D_i^3}{\sum N_i} \right)^{1/3} \quad (4)$$

N is the number of drops measured, D_i is the diameter of the individual drops, PA is the probe cross sectional area, and t_{total} is the sample time. If these quantities are accurately defined or measured for both the small and large size range, the flux in the overlap region (between the vertical green and red lines) should agree as shown in Fig. 9. Since the flux is dependent on volumetric qualities, it requires a large number of drops to generate a smooth curve for the flux values. Although there are fluctuations, the mean flux in the overlap region is in good agreement, within +/-10%. The combined results are then used to compute the MVD and LWC values for the entire size distribution. An example is shown in Fig. 10 with the lowest histogram for the large size range, the middle for the small size range, and the upper histogram and cumulative results are for the combined data.

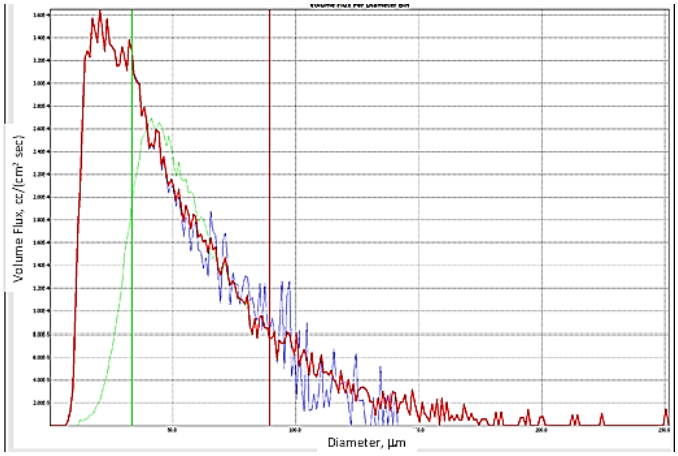

Figure 9: Plot of the volume flux as a function of droplet diameter for the small (blue line) and large size (green line) ranges showing the agreement in the overlap region for the small and large size range measurements. The red line is the combined small and large size range result.

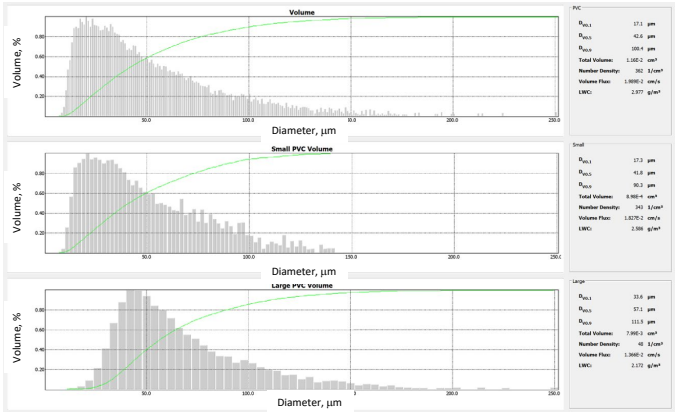

Figure 10: Percent volume histograms for the small and large size ranges and the combined result in the upper histogram.

Results and Discussion

As part of the instrument development program for SLD measurements, a series of tests were conducted in the NASA IRT [22]. These tests involved the Artium PDI FPDR and the Artium PI PTV (Particle Imaging system with Particle Tracking Velocimetry). A wide range of test conditions were covered including MVD values, LWC, and flow speed. In the following sections, selected examples of the measured results are presented.

The results in Fig. 11 are for the PDI small size range and are presented to show the effect of insufficient size range capability with a single measurement range. Agreement in the IRT calibration values of MVD was within +/-20% until approximately 50 µm. The measurements for

the small MVD values are higher than the IRT values due to either oversizing by the PDI FPDR or under-sizing by the CDP. Thereafter, the measured size decreases relative to the IRT calibrated results, since the largest drops in the spray distribution are not being measured. The large size range measurements shown in Fig. 12 provide relatively good agreement with IRT calibration MVD values but show a bias upward at the small end. This is due to the large size range not having sensitivity to the smallest drops in the size distribution. The combined size distribution shown in Fig. 13 captures the entire size distribution and shows that the merging of the small and large size distributions is reliable. The agreement with the IRT calibration results are within +/-15% with the exception of a few points. This exception is true for the smallest MVD values which are reported as higher by the PDI FPDR. A comparison of the drop size distributions acquired with the PDI FPDR and the PI PTV are shown in Fig. 14. The distributions are similar, but the cumulative results show a difference with the PDI FPDR indicating a higher MVD. A possible reason for the difference is that the PDI FPDR collected approximately 300,000 readings whereas the PI PTV collected approximately 10,000. The PDI FPDR provided a better statistical representation of the largest drops in the distributions.

Measurements of the LWC show some interesting results (Fig. 15), in which the LWC was plotted versus the IRT MVD values. The PDI FPDR measures the size and velocity of individual drops as well as the in situ measurement of the sample volume. The LWC is measured by calculating the volume of liquid drops within the swept volume defined by the sample volume area, the measured flow velocity, and the sample time. The calculation is the liquid flux, as stated in Equation 3 above, multiplied the water density divided by the flow velocity. For the smaller drops, the LWC measured by the PDI instrument was in relatively good agreement with the IRT calibration results up until approximately 100 µm. Thereafter, the PDI results showed an increasing difference with increasing MVD values. The particle imaging (PI PTV) results were added to this plot to help assess whether it was the IRT results or the PDI of measurements that were causing the differences. As seen in this plot, the PDI and PI PTV results, based on light scattering and particle imaging, respectively, show agreement of within +/-10% with a few points outside of this range, but diverge from the IRT results. A possible explanation of the differences in the LWC measurements may be due to the IRT measurements being based on impingement-based probes (multi-element sensor and icing blade results).

It is possible that droplet splashing occurs for the larger drops impacting these material devices [20]. It has also been postulated that evaporation may not be complete for the hotwire devices when attempting to measure larger drops [21]. Additional testing will be conducted to verify these results and to continue the validation and evaluation of these measurement methods for SLD conditions.

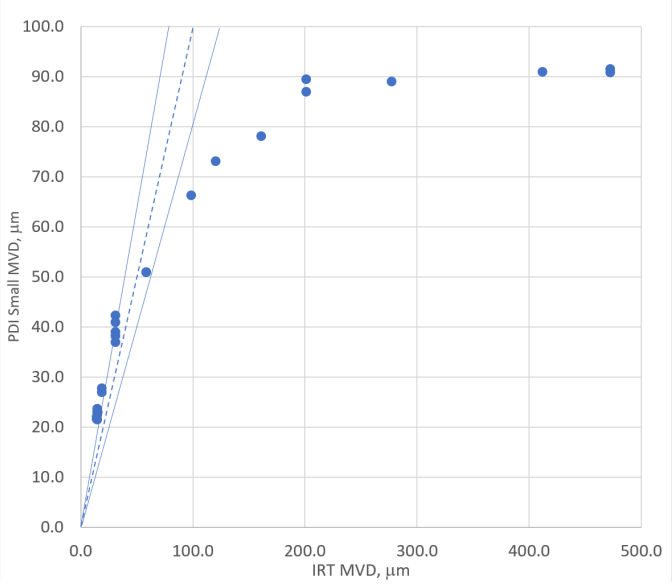

Figure 11: SLD data for PDI FPDR measurements with only the small size range, PDI Small. For MVD values larger than 50 µm, large drops were not captured by the small size range. Lines shown are at +/-20%.

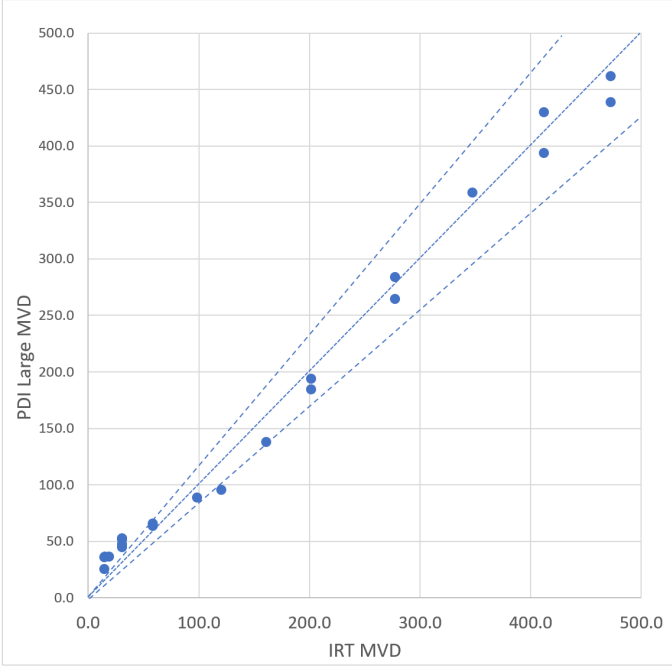

Figure 12: SLD data for the PDI FPDR measurements with only the large size range. In this case, the largest drops were measured but the smallest drops were below the detection limit. Larger MVD values for the small sizes were biased upward because of the lower size limit of the large size range channel. Lines indicate +/-15% of the IRT calibration results.

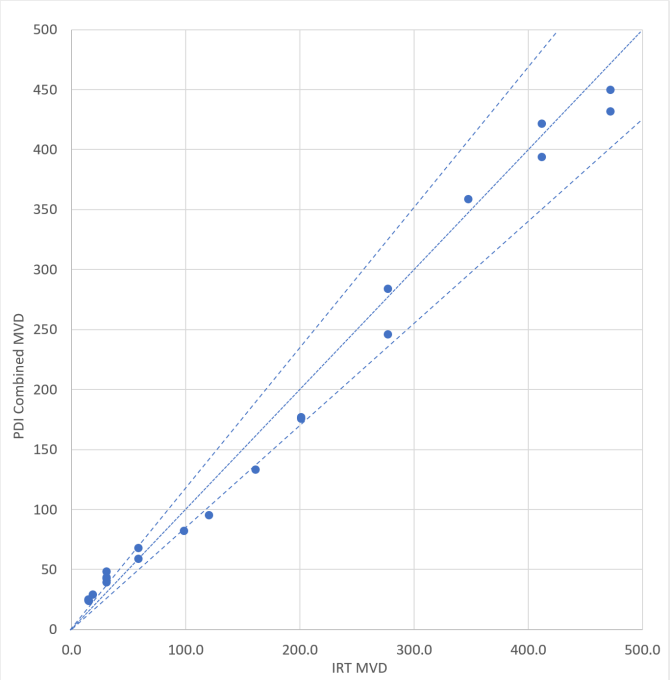

Figure 13: Data acquired with the PDI FPDR showing the combined results for the small and large size ranges for the SLD tests, all data. Note that the MVD results for the smallest drops are consistently high for both the small size range and the combined. The lines are at +/-15% 0f the IRT calibration results.

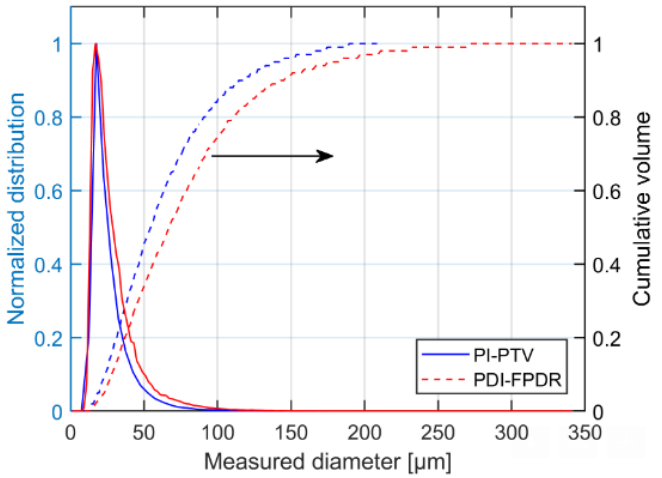

Figure 14: Examples of the size distributions measured by the PDI FPDR and the PI PTV droplet imaging instrument. The PDI instrument reports a slightly larger size than the PI PTV instrument.

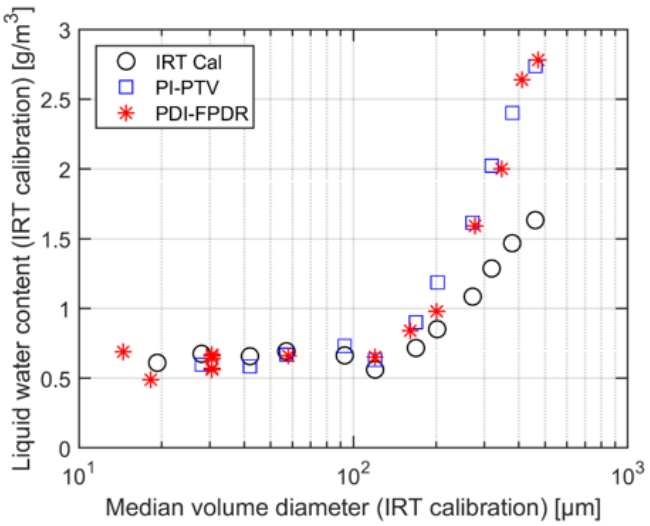

Figure 15: Plot of the LWC results for the PDI Large, PI PTV, and IRT versus the IRT MVD calibrated values.

Summary and Conclusions

In this report, a brief description of the phase Doppler interferometry method was provided. The method has the advantage of allowing measurements over a very wide size range but with dynamic range limited to approximately 50 to 1 in drop size. Furthermore, to accommodate this large working range, optics must be designed to accommodate the prevailing drop size conditions. In principle, a single optical configuration could accommodate the entire droplet size range of from 1 to 2200 µm. However, other constraints need to be addressed. Even with more powerful lasers (1000 mW), the beam diameter is limited by the need for sufficient light scatter by the smallest drops. A greater constraint is due to particle coincidence (more than one particle in the sample volume at one time). In the current approach, two PDI instruments with two separate measurement ranges have been built into one compact aerodynamic package. The small and large size ranges were designed to accommodate drop size ranges of 1 to 150 and 50 to 2200 µm with appropriate optical parameters. Drops will arrive randomly with arrival rates that can be described by Poisson statistics. A basic analysis showed that coincidence is inevitable but with probabilities dependent upon droplet number density and the sample volume size. To deal with this condition, a signal parsing approach has been implemented that mitigates but does not eliminate the problem.

Experiments were conducted in the NASA IRT with a wide range of conditions including SLD. Sample measurements showed good agreement with the IRT MVD results. LWC measurements were in agreement for small values of MVD but diverged significantly for larger values. Comparisons of LWC measurements between the PDI method with the particle imaging data were within 10% with a few exceptions. Additional tests will be conducted as the instrumentation are refined.

References

1. Knollenberg, R.G., “Three New Instruments for Cloud Physics Measurements: The 2-D Spectrometer, the Forward Scattering Spectrometer Probe, and the Active Scattering Aerosol Spectrometer,” American Meteorological Society, Intnl Conference on Cloud Physics, July, 1976, pp.544-561.

2. Miller, D., Ratvasky, T., Bernstein, B, McDonough, F., and Strapp, J.W., 1998: “NASA/FAA/NCAR Supercooled Large Droplet Icing Flight Research: Summary of Winter 96-97 Flight Operations”. AIAA 36th Aerospace Sci. Meeting and Exhibit, Reno, Nevada, AIAA Paper 98-0577.

3. Bellucci, M., Vernillo, P., Auletta, A., Esposito, B.M., Marrazzo, M., and Ferrigno, F., -SONACA Icing test campaign on a 2D model at CIRA IWT–SAE 2007-01-3335-SAE 2007 Aircraft & Engine Icing International Conference.

4. King, M. C., Bachalo, W. D., Bell, D., and King-Steen, L. E., “Weber Number Tests in the NASA Icing Research Tunnel,” *2018 AIAA Atmospheric and Space Environments Conference*, American Institute of Aeronautics and Astronautics, Atlanta, GA, AIAA 2018-3184.

5. De Gregorio, F., Esposito, B.M., Mingione, G., and Vicini, A., “Experimental and Computational Aerodynamics Applications for an Icing Wind Tunnel Design”, AGARD fluid dynamics panel symposium on “Aerodynamic of Wind Tunnel Circuits and their Components”, AGARD-CP-585, October 1996 Moscow.

6. Bond H.T., Miller, R.D., Potapczuk M.G., “Overview on SLD Engineering tools development”, AIAA 41st Aerospace Sci. Meeting and Exhibit 2003, Reno, Nevada, AIAA Paper 03-0386.

7. “Quality Assessment for Wind Tunnel Testing”, AGARD Advisory Report No. 304, July, 1994.

8. “Assessment of Experimental Uncertainty With Application to Wind Tunnel Testing’, AIAA Standard S-071A-1999, May, 1999.

9. “Calibration and Acceptance of Icing Wind Tunnels”, SAE-ARP 5905.

10. Lance, S., “Coincidence errors in the cloud droplet probe (CDP) (TAS), and the improved performance of the modified CDP,” J.Atmos. Ocean. Technolg., 29, 1532-1541, doi:10.1175/JTECH-d-11-00208.1, 2012.

11. Faber, S., French, J.R., and Jackson, R., “Laboratory and In-Flight Evaluation of a Cloud Droplet Probe (CDP),” Atmos. Meas. Tech. Discuss., https://doi.org/10.5194/amt-2017-479.

12. Korolev, A.V., Strapp, J.W., and Isaac, G.A., “Evaluation of the accuracy of PMS optical array probes”. J. Atmos. Oceanic Tech., 15, 708-720, 1998.

13. Strapp, J.W., Albers, F., Reuter, A., Korolev, A.V., Maixner, U., Rashke, E., and Vukovic, Z., “Laboratory Measurements of the Response of a PMS OAP-2DC”. J. Atmos. Oceanic Technol., 18,1150-1170, 2001.

14. Bachalo, W.D., “A Method for Measuring the Size and Velocity of Spheres by Dual Beam Light Scatter Interferometry,” Appl. Opt. 19 363-370 (1980).

15. Bachalo, W.D. and Houser, M.J. "Phase Doppler Spray Analyzer for Simultaneous Measurements of Drop Size and Velocity Distributions," Opt. Eng. 23, 1984, 583-590.

16. Bachalo, W.D., and Ibrahim, K.M., U.S. Patent 5,289,391, Feb. (1994).

17. Bachalo, W.D., Ibrahim, K.M., and Payne, G.A., U.S. Patent 7,564,564, July, (2009).

18. Bachalo, W.D., Rudoff, R.C., and Brena de la Rosa, A., "Mass Flux Measurements of a High Number Density Spray System Using the Phase Doppler Particle Analyzer", Presented at the AIAA 26th Aerospace Sciences Meeting, Reno, Nevada, January 11-14, 1988.

19. Bachalo, W.D., Payne, G.A, and Ibrahim, K.M., “Advances in the Phase Doppler Method for Dense Spray Measurements,” ILASS-Americas 29th Annual Conference on Liquid Atomization and Spray Systems, Atlanta, GA, May 2017.

20. Miller, D. R., Lynch, C. J., and Tate, P.A., “Overview of High Speed Close-up Imaging in an Icing Environment,” NASA/TM, 2004-212925, AIAA -2004-0407.

21. Wendisch, M., “A quantitative comparison of ground-based FSSP and PVM measurements,” Journal of Atmospheric and Oceanic Technology, Vol. 15, No. 4, pp. 887-900, 1998.

22. Van Zante, Judith, Strapp, J.W., Esposito, B., Orchard, D., Korolev, A., Ratvasky, T. and Riley, J., “SLD Instrumentation in Icing Wind Tunnels – Investigation Overview”, *2021 AIAA Aviation Forum*, virtual, AIAA-2021-2647, August 2021. doi: 10.2514/6.2021-2647.

Contact Information

William D. Bachalo, Ph.D.
Artium Technologies, Inc.
wbachalo@artium.com

Acknowledgements

The authors gratefully acknowledge the support of NASA Glenn Research Center and DOE under their SBIR Phase I and II programs. We acknowledge the significant contributions of the operational staff of the NASA Icing Research Tunnel. We thank Dr. Judith Van Zante for her guidance and support of the test conditions.

Definitions/Abbreviations

DPSS	diode pumped solid state
DMT CDP	Droplet Measurement Technologies Cloud Droplet Probe
FAA	Federal Aviation Administration
FSSP	forward scattering spectrometer probes
LWC	liquid water content

MVD	median volume diameter
NASA IRT	National Aeronautics and Space Administration Icing Research Tunnel
OAP	optical array probes
PDI FPDR	Phase Doppler Interferometer, Flight Probe Dual-Range
PI / PI PTV	Particle Imaging system with Particle Tracking Velocimetry
PV	probe volume
SLD	super-cooled large drops
SNR	signal-to-noise ratio